Journal of Scientific Computing, Vol. 17, Nos. 1–4, December 2002 (© 2002)

A Reduced-Basis Element Method

Yvon Maday[1] **and Einar M. Rønquist**[2]

Received November 22, 2001; accepted (in revised form) December 3, 2001

Reduced basis methods are particularly attractive to use in order to diminish the number of degrees of freedom associated with the approximation of a set of partial differential equations. The main idea is to construct ad hoc basis functions with a large information content. In this note, we propose to develop and analyze reduced basis methods for simulating hierarchical flow systems, which is of relevance for studying flows in a network of pipes, an example being a set of arteries or veins. We propose to decompose the geometry into generic parts (e.g., pipes and bifurcations), and to contruct a reduced basis for these generic parts by considering representative geometric snapshots. The global system is constructed by gluing the individual basis solutions together via Lagrange multipliers.

KEY WORDS: Partial differential equation; reduced basis; geometric snapshot; spectral element; nonconforming.

1. INTRODUCTION

Reduced basis methods (see [5]) are particularly attractive to use in order to diminish the number of degrees of freedom associated with the numerical approximation to a set of partial differential equations; the computational complexity can be reduced to a level where potentially very complex systems can be simulated, or where highly repetitive use of the underlying model becomes feasible, e.g., for design, optimization and real time control. The main idea is to construct basis functions with a large information content in order to reduce the number of basis coefficients needed to reach a certain level of accuracy in the outputs of interest.

The reduced basis approach is founded on the fact that many problems can be cast in the following form: for a given value of μ, find $u(\mu) \in X$ such that

$$F(u(\mu); \mu) = 0 \tag{1}$$

[1] Laboratoire d'Analyse Numérique, Université Pierre et Marie Curie, Boîte courrier 187, 75252 Paris Cedex 05, France.

[2] Department of Mathematical Sciences, Norwegian University of Science and Technology, N-7491 Trondheim, Norway. E-mail: ronquist@math.ntnu.no

0885-7474/02/1200-0447/0 © 2002 Plenum Publishing Corporation

where X is some functional space, the parameter μ (e.g., representing material properties, geometric parameters, time, or some control) belongs to some subset of $\mathbb{R}^p$, and F is a given mapping defined over $X \times \mathbb{R}^p$. The basic idea of the reduced basis method is that, as a function of the parameter μ, the solution $u(\mu)$ is often a very nice function so that, provided that some realizations $u(\mu_i)$ are known for some values $\mu = \mu_i$, with $i = 1,\ldots, n$, then by interpolation or extrapolation, we can predict a good approximation of $u(\mu)$ for a generic value of μ. In order to choose, among the many possibilities for inter- or extra-polation, a Galerkin method is most often involved since for many types of problems, it allows us to infer the best linear combination of the various $u(\mu_i)$.

The reduced basis methods are very attractive since, with very few basis functions, they describe the solution very well for many values of μ. However, these methods can also be deceptive because the computation may involve too few basis functions to approximate the solution sufficiently well over the entire parameter space of interest; note that *a priori* information about the correct and minimal number of basis functions is, of course, not available. The reduced basis approach and the associated recent definition of bounds for outputs of interest are two coherent tools that allow us to extend the domain of applicability of numerical simulation by both increasing the speed of the computations and by providing conservative error bars on the outputs (see [4] and [6]).

So far, the use of such reduced basis methods has been limited to finite dimensional parameter spaces. In the POD method, for evolution problems (see [1] and [3]), time has been used as a parameter, and the solutions are found as linear combinations of snapshots of the process. Our approach here is to understand to what extent one can use the geometry of the computational domain as a generic parameter. We think of using "geometric snapshots" to approximate generically new situations. The purpose of this paper is to demonstrate the feasibility of taking the geometry as a parameter. We shall propose in a future work the associated bounds for outputs.

In order to define our approach in more detail, we focus on geometries which can be decomposed into relatively simple parts, but where the overall system may be complex. An example of such a system is the flow in a network of pipes that can easily be decomposed, through a nonoverlapping domain decomposition, into a few generic shapes like deformed pipes and deformed bifurcations. The overall network is then comprised of the assembly of these simple generic parts, hereafter called elements, and each of these elements are provided with a family of generic solutions. Our objective is to glue together both the shapes and the functions using Lagrange multipliers (in a mortar-like approach as explained in [2]). This allows us to define global functions by which we shall approximately solve the global problem.

This paper is a presentation of the first results we have obtained together with some heuristic analysis. We think that these results indicate that the proposed "reduced-basis element" method appears to have a

potential interest. The particular PDE will be the Laplace equation, but this may already provide some hints to the behaviour of fluids through potential flow analysis.

2. DEFINITION OF THE APPROACH

We consider first the Poisson problem in a two-dimensional domain Ω with f given in $L^2(\Omega)$: find $u \in H^1(\Omega)$ such that $-\Delta u = f$ in Ω, complemented with appropriate boundary conditions.

We assume that the domain Ω can be decomposed into a nonoverlapping union of subdomains Ω_k, $k = 1,..., K$, such that each Ω_k is obtained as the deformation of a reference polygonal shape by a regular one to one transformation Φ_k. The reference shape will either be a square $]-1, 1[^2$ or a reference bifurcation. In general, we denote these reference shapes as $\mathscr{B}^m$, $m = 1,..., M$, and we assume that M is very small; here, we consider $M = 1$ or $M = 2$ for the sake of simplicity. Each Ω_k is thus a deformation of some $\mathscr{B}^{m(k)}$. We also make the assumption of "geometrical conformity" in the sense that each interface $\Gamma_{k,\ell}$ between two adjacent subdomains Ω_k and Ω_ℓ is assumed to be a whole common side of both Ω_k and Ω_ℓ (a side of Ω_k is, of course, a curved side that is the image of one side of the reference polygonal through the mapping Φ_k).

We assume further that each reference domain $\mathscr{B}^m$ comes with a set of functions w_i^m, $i = 1,..., I$, so that, over Ω, a finite dimensional space can be introduced:

$$Y_\delta = \{v \in L^2(\Omega),\ v_{|\Omega_k} \circ \Phi_k \in \mathrm{Vect}\{w_i^{m(k)}\}\} \tag{2}$$

In order to propose an admissible discrete space for $H^1(\Omega)$, we have to glue together the values of elements of Y_δ through each interface $\Gamma_{k,\ell}$. The exact coincidence of the traces of the discrete functions is generally too stringent, and may, in fact, lead to imposing $v = 0$ on the interface; thus, the gluing process is done in a dual way through Lagrange multipliers. We denote by $W_{k,\ell}$ a set of functions over each interface $\Gamma_{k,\ell}$, and we define

$$X_\delta = \left\{ v \in Y_\delta,\ \forall k, \ell,\ \forall \psi \in W_{k,\ell},\ \int_{\Gamma_{k,\ell}} (v^+ - v^-)\,\psi = 0 \right\} \tag{3}$$

where, for a given v in Y_δ and any interface $\Gamma_{k,\ell}$, $v^+_{\Gamma_{k,\ell}} (= v^+)$ and $v^-_{\Gamma_{k,\ell}} (= v^-)$ stand for the two values that v takes on each side of $\Gamma_{k,\ell}$. Of course, the approximation space is generally not a subspace of $H^1(\Omega)$ and the method is nonconforming. The definition of the Lagrange multiplier space $W_{k,\ell}$ has to be done in a proper way and can also be defined through a mapping from a reference space of test functions over $]-1, 1[$. If we assume that $\chi_{k,\ell}$ is a parametrization from $]-1, 1[$ onto $\Gamma_{k,\ell}$, then a possible choice is $W_{k,\ell} = \{\psi \circ \chi_{k,\ell}, \psi \in \mathscr{W}_\delta\}$ where $\mathscr{W}_\delta$ is some given finite dimensional space.

The discrete problem can now be defined as: find $u_\delta \in X_\delta$ such that $\int_\Omega \nabla u_\delta \nabla v_\delta = \int_\Omega f v_\delta$ for all $v_\delta \in X_\delta$. It is an easy matter to check that this problem is well posed as soon as there exists a part of the boundary of Ω on which a Dirichlet boundary condition is imposed on u, and as soon as the constant functions belong to $W_{k,\ell}$, i.e., to $\mathscr{W}_\delta$. In addition, the following error estimate holds (known as the second Strang lemma)

$$\|u-u_\delta\|_* \leqslant c \inf_{v_\delta \in X_\delta} \|u-v_\delta\|_* + c \max_{v_\delta \in X_\delta} \max_{k,\ell} \frac{\int_{\Gamma_{k,\ell}} \dfrac{\partial u}{\partial n_{k,\ell}} (v^+ - v^-)}{\|v_\delta\|_*} \tag{4}$$

where in the last expression—known as the consistency error—$n_{k,\ell}$ stands for the normal to the interface $\Gamma_{k,\ell}$. The first term in this error estimate is known as the best fit error and its smallness relies on the approximation properties of the basis functions $w_i^{m(k)}$.

The smallness of the consistency terms relies on the orthogonality property indicated in (3) that allows us to write

$$\int_{\Gamma_{k,\ell}} \frac{\partial u}{\partial n_{k,\ell}} (v^+ - v^-) = \int_{\Gamma_{k,\ell}} \left[\frac{\partial u}{\partial n_{k,\ell}} - \psi \right] (v^+ - v^-)$$

It remains to choose a ψ in $W_{k,\ell}$ close enough to $\frac{\partial u}{\partial n_{k,\ell}}$. This remark helps us in choosing the space $\mathscr{W}_\delta$.

In contrast to general purpose methods such as finite element or spectral element methods, the evaluation of the best fit is not based on a density result formally written as $\overline{\bigcup_{\delta \to 0} X_\delta} = H^1(\Omega)$, but on the fact that $\{u(\mu), \mu \in \mathbb{R}^p\}$ is embedded in a low-dimensional manifold so that very few elements in this set may represent the whole manifold well. This is the main difference between a general purpose method and the reduced-basis element method: the dimension of the approximation space for the latter is much smaller, and the corresponding computational complexity is also smaller.

The previous definition of the space X_δ is general enough so that many methods fit into this framework. Our approach differs in the definition of the discrete functions w_i^m, $i = 1,\ldots, I$. These are obtained by solving the problem we are interested in (here the Laplace problem) in some snapshots of deformed geometries and then mapped back over $\mathscr{B}^m$. This is the basic idea that was introduced in the Introduction, and which will be detailed further in the next section.

3. DEFINITION OF THE BASIS FUNCTIONS IN ONE DOMAIN

In what follows, we assume that the domain Ω is the range of $]-1, 1[^2 = \mathscr{B}^1$ by a regular mapping Φ. The domain of interest is thus a

deformed square with 4 curved edges Γ_1, Γ_2, Γ_3 and Γ_4. We then consider the Laplace problem ($f = 0$): find $u \in H^1(\Omega)$ such that

$$-\Delta u = 0 \qquad \text{in } \Omega \tag{5}$$

with boundary conditions

$$u = 1 \text{ over } \Gamma_1, \qquad u = 0 \text{ over } \Gamma_3, \qquad \frac{\partial u}{\partial n} = 0 \text{ over } \Gamma_2 \text{ and } \Gamma_4 \tag{6}$$

Let us now describe the approach for defining the discrete basis functions w_i^1 over $\mathscr{B}^1$. We choose I geometric shapes, i.e., we choose I deformation mappings Φ_i from $\mathscr{B}^1$ into $\mathbb{R}^2$, and solve as accurately as possible the corresponding problems of the type (5). The resulting solutions are denoted as u_i and are mapped onto $\mathscr{B}^1$; we then set $w_i^1 = u_i \circ \Phi_i$.

Note that, for the non-homogeneous boundary condition in (6), we can proceed in two ways. One alternative is to keep all the precomputed solutions as they are, including their non-homogeneous essential boundary conditions. However, a linear combination must honor the essential boundary condition $u = 1$ over Γ_1.

Another alternative which is equivalent, but which affects the implementation, is to use one of the precomputed basis funtions (w_1^1, say) in order to take care of the non-homogeneous boundary condition; the remaining basis functions are then homogenized by subtracting off w_1^1. For all the numerical tests below, we have followed this latter approach.

As a simple numerical example, we consider the solution of the Laplace equation in a domain depicted in Fig. 1. The domain corresponds to one quarter of a complete annulus, i.e., a 90° bend; the inner radius is 2, while the outer radius is 3. As a reduced basis, we use the solution of the Laplace equation on a square, which is just a linear function for the type of boundary conditions considered in this problem; this basis function is also

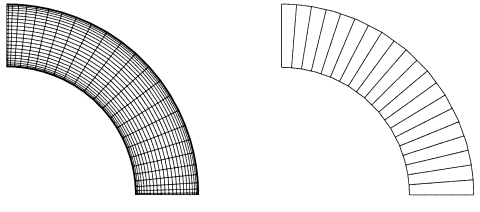

Fig. 1. The computational domain is here one quarter of a complete annulus (concentric circles intersecting straight lines at 90° angles); the inner radius is 2, while the outer radius is 3. A single spectral element is used to represent the computational domain as shown on the left; a Gordon–Hall algorithm is used to map the reference domain to the computational domain. Contours of the reduced basis solution to the Laplace equation is shown on the right; only a single, non-homogeneous basis function is used in this case, namely the solution to the Laplace equation on a square. The discrete solution is exact to essentially machine precision.

depicted as the first basis function in Fig. 2. In fact, this basis function will be used in all the subsequent numerical examples, and represents the non-homogeneous basis function.

As a more complicated example, we consider the solution of the Laplace equation in a deformed 90° bend; see Fig. 3. We choose mappings Φ_i, $i = 1,\ldots, I$ corresponding to deformed squares as well as other deformed 90° bends; see Fig. 2. In all cases, only the edges Γ_2 and Γ_4 are curved; the edges Γ_1 and Γ_3 are straight sides which are either parallel to each other or perpendicular to each other.

We now describe the analytical shapes of the deformed edges Γ_2 and Γ_4. The first 4 preselected geometries in Fig. 2 can generally be described as a

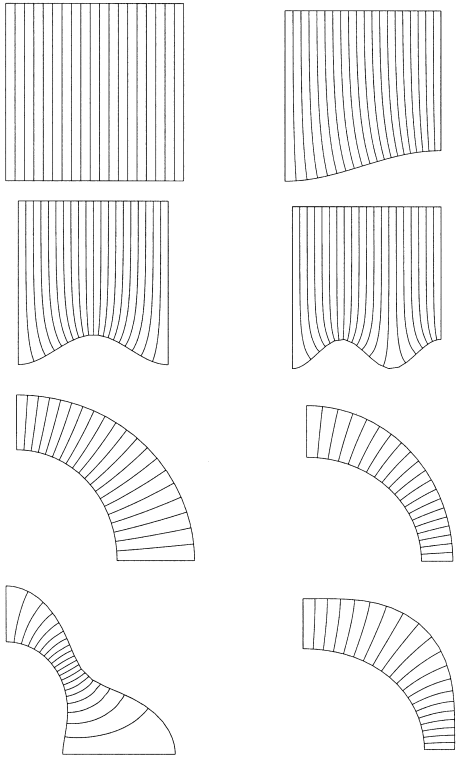

Fig. 2. Preselected geometries with contours of the precomputed solutions to the Laplace equation. Three of the geometries have a simple trigonometric deformation along the bottom side; symmetric variants of the corresponding solutions (corresponding deformations along the top side) are easily obtained. Note that the precomputed/preselected solutions are represented on the reference domain and mapped back to the computational domain of interest, either to the global domain or to a particular subdomain or element.

unit square with the bottom edge Γ_2 deformed only in the y-direction according to the functional form

$$\Delta y = a_2 \cdot \cos(\omega \pi x), \qquad 0 \leqslant x \leqslant 1 \tag{7}$$

For the first preselected geometry (the unit square), $a_2 = 0$, i.e., no deformation at all. For the following 3 preselected geometries, $a_2 = -0.1$, while $\omega = 1$, 2 and 3, respectively.

The last 4 preselected geometries in Fig. 2 correspond to taking the 90° bend depicted in Fig. 1, and deforming the sides Γ_2 and Γ_4 in both the x- and y-direction according to the following functional forms.

On Γ_2, the deformation from a pure annulus can be described as

$$\Delta x = b_2 \cdot (1 - \cos(2\theta)) \cdot \sin(\theta) \tag{8}$$

$$\Delta y = b_2 \cdot (1 - \cos(2\theta)) \cdot \cos(\theta) \tag{9}$$

while on Γ_4, the deformation from a pure annulus can be described as

$$\Delta x = b_4 \cdot (1 - \cos(2\omega\theta)) \cdot \sin(\theta) \tag{10}$$

$$\Delta y = b_4 \cdot (1 - \cos(2\omega\theta)) \cdot \cos(\theta) \tag{11}$$

Here, $0 \leqslant \theta \leqslant \pi/2$, and θ is increasing in the clockwise direction.

For the last 4 preselected geometries in Fig. 2, the following sets of parameter values (b_2, b_4, ω) are used: $(0.1, -0.1, 1.0)$, $(-0.1, 0.1, 1.0)$, $(-0.5, -0.5, 2.0)$, and $(0.2, 0.2, 2.0)$. The parameter values for the actual test case in Fig. 3 are $(-0.2, -0.3, 2.0)$.

All the preselected problems are discretized and solved using a single spectral element of order $p = 25$. Armed with a set of precomputed basis functions w_i^1, we compute a reduced-basis element solution and compare this solution with the precomputed "exact" solution. The maximum pointwise relative error, e, is reported in Table I as a function of the total number of basis functions. In conclusion, for the computational problem considered here, and for the particular mappings chosen, exponential convergence is obtained.

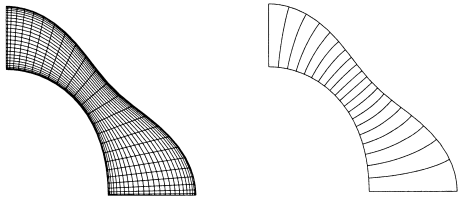

Fig. 3. Computational domain of interest. Spectral element discretization (left) and contours of the reduced basis solution to the Laplace equation (right). The basis functions correspond to the preselected geometries depicted in Fig. 2.

Table I

I	e
7	0.098
9	0.019
11	0.0058

It is of interest to understand to which extent this method enters within the framework of the reduced basis methods. Through a simple change of variable, problem (5) can be set over $\mathscr{B}^1$. Indeed, it takes the form $\int_{\mathscr{B}^1} \mathscr{J}(\Phi^{-1})\, \nabla\hat{u}\, \mathscr{J}(\Phi^{-1})\, \nabla\hat{v}\, J(\Phi)\, d\hat{x}\, d\hat{y} = \int_{\mathscr{B}^1} \hat{f}\hat{v}\, J(\Phi)\, d\hat{x}\, d\hat{y}$ where $\hat{v}$ stands for $v \circ \Phi$, $\mathscr{J}(\Phi^{-1})$ is the jacobian matrix Φ^{-1} and $J(\Phi)$ is the jacobian of Φ. The dependency of this problem on the shape Φ is thus made explicit, and the problem can be written in the form (1). We may thus consider Φ as a parameter and write $\hat{u} \equiv \hat{u}(\Phi)$. In addition, it is an easy matter to verify that, at least in the neighborhood of the identity mapping $\Phi = \mathrm{Id}$, the solution $\hat{u}(\Phi)$ together with $u(\Phi)$ are $\mathscr{C}^\infty$ functions of Φ. This allows us to predict a good approximation property of $\hat{u}(\Phi)$ by a linear combination of the w_i^1.

4. DEFINITION OF THE BASIS FUNCTIONS IN THE MULTI-DOMAIN CASE

For purposes of exposition, we revisit our sample problem from the previous section, but this time in the multi-domain case. We now need to generate basis functions with good approximation properties also at the level of the element interfaces. In addition, we would like to reuse our set of generic basis functions over similar parts (in our case, deformed pipes). In order to meet these objectives, our approach is as follows. As in the single-domain case, we compute reference solutions in preselected geometries Ω_i, but where the domains are obtained through the deformation of the rectangle $]-1, 3[\times]-1, 1[$. The basis functions w_i^1 are then chosen to be the restrictions of these computed solutions (mapped back over the rectangle) to $]-1, 1[^2$. This way, on the boundary $\{1\} \times]-1, 1[$—that corresponds to an interface, say—the shape of w_i^1 is not predefined.

In the numerical examples below, we will choose the same preselected geometries as in the single-domain case; see Fig. 2. However, instead of discretizing these domains using a single spectral element, we will use 2 spectral elements of approximately equal size. The precomputed solutions will be restricted to one of the two spectral elements, and these restricted solutions will be used to construct a reduced basis for the actual problem of interest.

The set of basis functions must be general enough to also be applicable to the case with two interfaces on a single element Ω_k (i.e., when $K \geqslant 3$). This can readily be achieved by using the precomputed set of basis func-

tions, and then add their symmetric variants over $]-1, 1[^2$; by using reflection with respect to both spatial directions, the constructed basis will also have reduced sensitivity to directional effects in the preselected mappings (or preselected deformed geometries). Another approach could be to define proper intermediate basis functions obtained similarly to w_1^1, but by retaining the values of u_i^1 over $]0, 2[\times]-1, 1[$. This way, on both boundaries $\{\pm 1\} \times]-1, 1[$, the shape of w_i^1 is not predefined.

In the spirit of the mortar spectral element method (see [2]), we choose here the Lagrange multiplier space $W_{k,\ell}$ to be the space of polynomials of degree less than or equal to n, with $n < p$.

Let us now return to the computational domain depicted in Fig. 3, but this time using 3 subdomains. The corresponding spectral element grid is depicted in Fig. 4, together with a contour plot of the solution and the error in the case of using $(14+28+14)$ homogenized basis functions in the 3 subdomains. The particular basis functions are based on the preselected geometries depicted in Fig. 2 (following the procedure explained above). One of the associated precomputed solutions, namely the solution to the Laplace equation on a square, is used to take care of the non-homogeneous boundary condition in the first element. The remaining 7 precomputed solutions in Fig. 2 are reflected in order to enrich the basis and reduce directional effects. This gives us a total of $2 \cdot 7 = 14$ homogenized basis functions which can be used directly in the last element, while the reflected versions are used in the first element. In the middle element, we use the full set of symmetrized and reflected basis functions.

In Fig. 4, we notice tendencies to wiggles in the reduced-basis solution within the first element. The contour plot of the error also indicates that most of the error is located around the first element. This is related to the fact that the interface between the first and second element intersects the curved boundaries at angles which are not 90°. In contrast, all the preselected geometries and their 2-element decompositions involve (deformed) elements with right corners. Hence, the right corners in the reference domain map to right corners in the preselected geometries. This fact makes the contructed basis less suitable to deal with computational domains which do not adhere to this restriction.

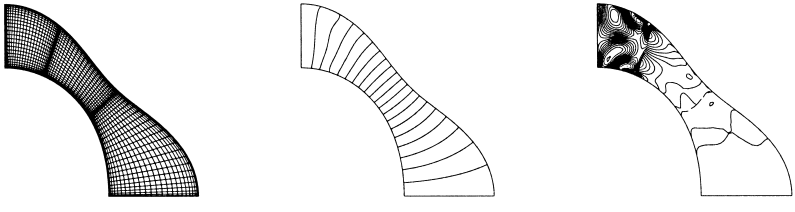

Fig. 4. (a) Three-domain case and associated spectral element grid; (b) contours of the reduced-basis solution; (c) error contours using $(15+28+14)$ basis functions and $n = 3$. The maximum pointwise error is $e = 0.0064$.

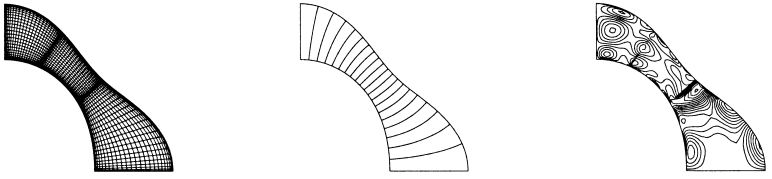

Fig. 5. (a) Three-domain case and associated spectral element grid; the 90° property is now approximately satisfied; (b) contours of the reduced-basis solution; (c) error contours using $(15+28+14)$ basis functions and $n=3$. The maximum pointwise error is $e=0.00060$.

One way to reduce the error in Fig. 4 is to contruct a new decomposition which comprise elements with 90° corner angles. Figure 5 shows a decomposition which approximately has this property. As expected, the associated error is now reduced compared to the results in Fig. 4; in fact, an order of magnitude reduction is observed.

Of course, we would like to be able to use decompositions where the individual elements do not necessarily conform to the 90° property. In order to improve the results in Fig. 4, we enrich the basis by solving the Laplace problem in the 2-domain case depicted in Fig. 6. Again, only the solution restricted to one of the elements is actually used.

We proceed with constructing a new reduced basis based on the last 4 preselected geometries in Fig. 2 plus the new one indicated in Fig. 6. Again, we include their symmetric variants, giving a total of 10 homogenized basis functions. For the internal element, we also reflect the 10 basis functions. With $(11+20+10)$ basis functions in the 3 subdomains, and $n=3$ ($n \ll p$), the maximum pointwise error is $e=0.0017$. This is about a factor 4 less than the error for the $(15+28+14)$ case from Fig. 4. Hence, we have decreased the error using a smaller but better set of basis functions.

From Fig. 7, we notice that the error appears to be located mainly at the level of the interfaces. This reveals that the choice of (low order) polynomials ($n=3$) is not completely appropriate, and that we should better define a space of Lagrange multipliers based on snapshots of $\frac{\partial u}{\partial n}$.

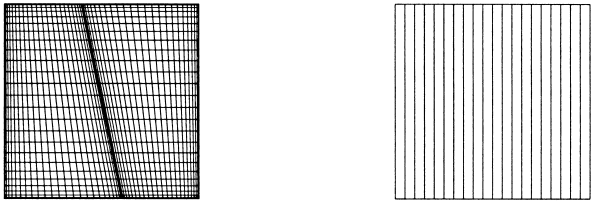

Fig. 6. Preselected geometry and spectral element discretization (left) in order to avoid the constraint of having the subdomain interfaces always intersect the curved boundaries at right angles. Contours of the precomputed solution to the Laplace problem (5)–(6) is shown on the right. Note that only the part of the solution which is restricted to a single spectral element, and mapped back to the reference domain, is actually used as a reduced basis function.

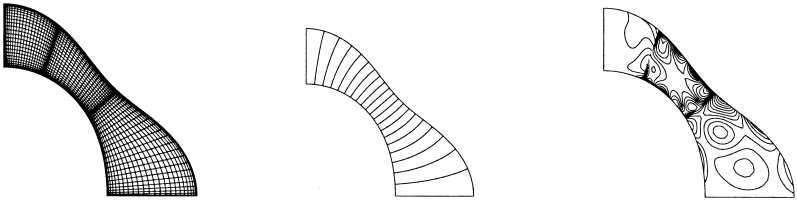

Fig. 7. (a) Three-domain case and spectral element grid; (b) contours of the reduced-basis solution; (c) error contours using $(11+20+10)$ basis functions and $n=3$. The maximum pointwise error is $e=0.0017$.

As a final example, we consider the "French horn" depicted in Fig. 8. Again the problem consists of solving the Laplace equation with boundary conditions specified in (5). In this case, 6 elements are used.

5. COMPLEXITY ANALYSIS

The computational cost associated with the reduced-basis element method comprises the cost of performing the following operations: (i) precomputing the functions w_i^m for each generic part m; (ii) constructing the reduced-basis element stiffness matrix and the associated right hand side; (iii) solving for the basis coefficients.

Step (i) can be done off-line using potentially a non-scalable or non-optimal simulation tool; the important thing is that the reduced order basis can be precomputed and stored for future use.

The cost of Step (ii) depends on the dimension of the reduced basis system. For the multi-domain case considered in Section 4, the dimension of the reduced-basis stiffness matrix is bounded by $K \times I + (K-1)(n+1)$; the dimension is essentially the number of basis functions for a particular

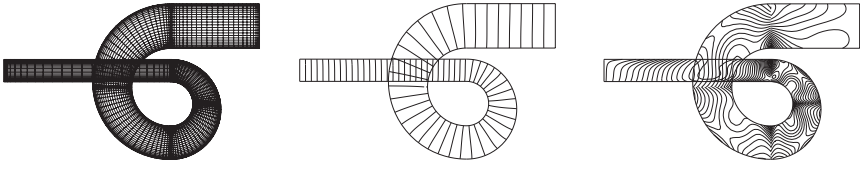

Fig. 8. The computational domain (a caricature of a French horn) is decomposed into 6 subdomains, and each subdomain is approximated by a single spectral element of order $p=25$. Instead of computing the associated spectral element solution in a standard fashion, we use the last 4 precomputed solutions in Fig. 2, together with their mirror image for internal elements, as a (homogenized) reduced basis within each element. The total number of basis functions used to represent the global solution is therefore $\dim(Y_\delta) = 5+8+8+8+8+4 = 41$. However, $\dim(X_\delta) = 31$ because of the 2 matching conditions associated with each of the 5 subdomain interfaces (here, $n=1$). The last figure shows the error contours; the maximum pointwise error (both absolute and relative) is $4.9 \cdot 10^{-3}$.

part (a pipe or a bifurcation) times the number of parts, plus the number of interface constraints associated with the subdomain interfaces.

Assume further that each discrete basis function $w_i^m(k)$ can be represented as a vector of dimension N (here, $N=(p+1)^2$). Overall, for the spectral element systems considered here, and with $p>I$, the total cost is dominated by the cost of constructing the reduced-basis element stiffness matrix for each element Ω_k, i.e., performing I global matrix-vector products.

If $\dim(X_\delta)$ is reasonably small, the simplest and best way to solve for the basis coefficients is to use a standard LU-decomposition, and the cost of Step (iii) is subdominant to the cost of Step (ii).

The global cost is thus dominated by the construction of the stiffness matrix. Through the use of tensorization, the global evaluation of each element of the stiffness matrix $\int_\Omega \nabla w_i \nabla w_j$ for any couple of elements of the reduced basis can be done in less than $c^* I p^3 + I^2 p^2/2$ operations, with a constant c^* which is known. Indeed, writing the vectors w_i in the polynomial basis leads to a p^2 vector $\underline{w}_i$. The value of $\int_\Omega \nabla w_i \nabla w_j$ is then expressed as $\underline{w}_i^T \underline{A} \underline{w}_j$ where $\underline{A}$ is the discrete Laplacian. We first compute the matrix-vector products $\underline{v}_j = \underline{A}\underline{w}_j$, $j=1,\ldots,I$. Next, we compute the innerproducts $\underline{w}_i^T \underline{v}_j$ for $i,j=1,\ldots,I$, where in the symmetric case, we only need about $I^2/2$ innerproducts.

The cost associated with our method has to be compared with the cost required to solve the set of algebraic equations resulting from applying the standard spectral element method to the same mapping (and possibly domain decomposition) of the domain Ω. It is well known that the spectral element solution is most often computed through a preconditioned iterative procedure that leads to a complexity equal to the number of iterations (say $\mathscr{I}$) times the evaluation of the residual, i.e., $c^* \mathscr{I} p^3$. The number of iterations, even with the best preconditioners available is—may be—independent of the polynomial order or the number of subdomains, but is generally unknown, and may be large for complex problems. One interesting attribute with the proposed method is that it has the potential of having a more predictable complexity.

6. FUTURE WORK

Future work will focus on three central aspects of the proposed methodology. The first one is the question of how to choose the geometric snapshots in order to ensure good approximation properties in the case of more general domains/parts and boundary conditions.

The second aspect is related to the reuse of the same set of basis functions for similar parts. When extending the proposed methodology to fluid flows, the complexity of the physics could have an impact on which set of basis functions would be the best choice for a particular part. We expect that this could be an issue for convection-dominated flows.

Finally, if the discrete approach maintains its appealing properties, the next step will be to derive *a posteriori* tools in order to provide confidence in the numerical results and in order to allow us to use the proper number of basis functions over each generic element (see [4] and [6]).

ACKNOWLEDGMENTS

We want to thank Olivier Pironneau for accepting a preliminary version of this paper as a note in the Compte Rendu de l'Académie des Sciences de Paris.

REFERENCES

1. Berkooz, G., Holmes, P., and Lumley, J. L. (1993). The proper orthogonal decomposition in the analysis of turbulent flows. *Ann. Rev. Fluid Mech.* **25**, 539–575.
2. Bernardi, C., Maday, Y., and Patera, A. T. (1990). A new nonconforming approach to domain decomposition: The mortar element method. In Brezis, H., and Lions, J. L. (eds.), *Nonlinear Partial Differential Equations and Their Applications*, College de France seminar, Pitman.
3. Christensen, E. A., Brøns, M., and Sørensen, J. N. (2000). Evaluation of proper orthogonal decomposition-based techniques applied to parameter-dependent nonturbulent flows. *SIAM J. Sci. Comput.* **21**(4), 1419–1434.
4. Machiels, L., Maday, Y., Oliveira, Y., Patera, A. T., and Rovas, D. V. (2000). Output bounds for reduced-basis approximations of symmetric positive definite eigenvalue problems. *C. R. Acad. Sci. Paris, Série I* **331**(2), 153–158.
5. Noor, A. K., and Peters, J. M. (1980). Reduced basis technique for nonlinear analysis of structures. *AIAA J.* **18**(4), 455–462.
6. Prud'homme, C., Rovas, D. V., Veroy, K., Machiels, L., Maday, Y., Patera, A. T., and Turinici, G. Reliable real-time solution of parametrized partial differential equations: Reduced-basis output bound methods. *J. Fluids Engineering*, to appear.